PHOFEX Spectroscopy of HgNe and HgAr: Determination of the Dissociation Energies of the $X^1\Sigma^+$, $A^3\Pi_{0^+}$, and $B^3\Pi_1$ States

Tomoki Tasaka, Ken Onda,# Akiyoshi Hishikawa, and Kaoru Yamanouchi*

Department of Pure and Applied Sciences, College of Arts and Sciences, The University of Tokyo, 3-8-1 Komaba, Meguro-ku, Tokyo 153

(Received January 8, 1997)

Photofragment excitation (PHOFEX) spectroscopy was applied to determine the dissociation energies of the $B^3\Pi_1$ states of HgAr and HgNe. The PHOFEX spectra were measured in the wavelength region where the laser-induced fluorescence spectrum of the $B^3\Pi_1$–$X^1\Sigma^+$ transition exhibits a continuum structure by probing the photolysis product of $Hg(6^3P_1)$ through the $Hg(8^3S_1$–$6^3P_1)$ transition. By the spectral simulation of the threshold behavior of the high-resolution ($\Delta\nu\approx0.08$ cm^{-1}) PHOFEX spectrum, the thresholds for the photodissociation reaction, HgRg→$Hg(6^3P_1)$+Rg, were determined to be 39447.9(3) and 39536.0(5) cm^{-1} for Rg = Ne and Ar, respectively. From these thresholds, the dissociation energies, D_0's, of the $B^3\Pi_1$ states of HgNe and HgAr were determined to be $D_0(B^3\Pi_1$; HgNe) = 9.8(3) and $D_0(B^3\pi_1$; HgAr) = 61.8(5) cm^{-1}, respectively. This direct determination of the dissociation energies of the $B^3\Pi_1$ states led to a determination of the D_0's for the $X^1\Sigma^+$ and $A^3\Pi_{0^+}$ states; $D_0(X^1\Sigma^+$; HgNe) = 35.6(3), $D_0(X^1\Sigma^+$; HgAr) = 123.7(5), $D_0(A^3\Pi_{0^+}$; HgNe) = 68.7(3), and $D_0(A^3\Pi_{0^+}$; HgAr) = 348.8(6) cm^{-1}. In addition, the $(v',0)$ vibronic bands of the $B^3\Pi_1$–$X^1\Sigma^+$ transition of HgAr were re-measured with high resolution for $v'=0$—8. From the transition wavenumbers of these vibronic bands, the Morse potential parameters were determined with high precision as $\omega_e = 11.94(3)$ cm^{-1} and $\omega_e x_e = 0.594(3)$ cm^{-1}.

Since the first observation of HgRg (Rg = a rare gas atom) diatomic van der Waals clusters produced in a supersonic jet by Fuke, Kaya, and co-workers,[1,2] the electronically excited states of the $HgRg_n$ (n=1,2,$\cdots$) clusters have been intensively investigated.[3—17] Recently, the investigation of HgRg clusters was systematically extended towards the highly excited region in order to understand the vibrational and dissociation dynamics in the Rydberg states.[11,18—22] In these studies, the interatomic potentials of HgRg in the low-lying electronic states ($X^1\Sigma^+$, $A^3\Pi_{0^+}$, and $B^3\Pi_1$) always played an important role. For determining of the dissociation energies in the Rydberg states, the dissociation energy for the electronic ground $X^1\Sigma^+$ state is required; also, for the interpretation of the intensity pattern observed in the optical–optical double resonance (OODR) spectrum, knowledge concerning the shape of the intermediate potentials, i.e. the $A^3\Pi_{0^+}$ and $B^3\Pi_1$ states, was crucial. Furthermore, the precise shape of the potential function of the $B^3\Pi_1$ state would facilitate an understanding of the dissociation reaction proceeding through the repulsive part of the $B^3\Pi_1$ state.

The previous spectroscopic studies showed that the vibrational level energies of the $A^3\Pi_{0^+}$ and $B^3\Pi_1$ states of the HgRg dimers were well described in terms of the Morse parameters (ω_e and $\omega_e x_e$). Since it has been known that the Morse potential approximation is not always appropriate, especially in the highly excited region near to the dissociation limit, the dissociation energies of the electronically excited $A^3\Pi_{0^+}$ and $B^3\Pi_1$ states of HgRg have relatively large uncertainties. Of course, if the dissociation energy (D_0'') of the electronic ground $X^1\Sigma^+$ state is known, D_0' for the electronically excited $A^3\Pi_{0^+}$ or $B^3\Pi_1$ state can be derived straightforwardly using the $6^3P_1 \leftarrow 6^1S_0$ transition wavenumber of Hg,[23] $\nu(Hg) = 39412.30$ cm^{-1}, as

$$D_0' = D_0'' + \nu(Hg) - \nu_{00}(HgRg), \quad (1)$$

where $\nu_{00}(HgRg)$ represents the band origin (v', v'')=(0,0) transition of the $A^3\Pi_{0^+}$–$X^1\Sigma^+$ or $B^3\Pi_1$–$X^1\Sigma^+$ band of HgRg. However, only an indirect estimate has been made of the dissociation energies (D_0''s) for the electronic ground $X^1\Sigma^+$ states of HgRg. Therefore, in order to solve this problem of persistent ambiguities in the dissociation energies of the low-lying electronic states of HgRg, it is necessary to determine the dissociation energy of one of these three electronic states. Once the dissociation energy of one of these electronic states is determined, those for the other two states can be derived using Eq. 1.

In the present study we introduced a technique of photofragment excitation (PHOFEX) spectroscopy in order to determine the dissociation energies (D_0's) of the $B^3\Pi_1$

Present address: Research Laboratory of Resources Utilization, Tokyo Institute of Technology, Nagatsuda, Midori-ku, Yokohama 226, Japan.

states of HgNe and HgAr with high-precision. This, in turn, led to the precise determination of the dissociation energies of both the $A^3\Pi_{0^+}$ and $X^1\Sigma^+$ states of HgNe and HgAr. PHOFEX spectroscopy is a variation of pump-and-probe type spectroscopy, in which the wavelength of the excitation laser causing the photodissociation is scanned while a specific quantum state of the photofragments is monitored by a second laser; this method has often been successfully applied to investigations of photodissociation reactions.[24—28] We demonstrate here that PHOFEX spectroscopy is efficient in determining the dissociation energy of the interatomic potentials of diatomic molecules in an electronically excited state when there is a sufficient Franck–Condon overlap between the electronic ground state and both the discrete and the continuum part of the potential in the electronically excited state. The PHOFEX spectrum for the $B^3\Pi_1$–$X^1\Sigma^+$ band of HgAr was previously measured by Quayle et al.[14] in order to estimate the rotational temperature of a free jet. However, no attempt has so far been made to determine the precise dissociation energies of the HgRg dimers by PHOFEX spectroscopy. We also report here on re-measurements of the high-resolution LIF spectrum of the $B^3\Pi_1$–$X^1\Sigma^+$ band of HgAr in order to determine the band-origin wavenumbers for the vibronic transitions, from which the Morse potential parameters (ω_e and $\omega_e x_e$) for the $B^3\Pi_1$ state of HgAr were determined with high precision.

Experimental

The van der Waals (vdW) dimers, HgNe and HgAr, were produced in a supersonic jet expanded into a vacuum chamber through a heated pulsed nozzle equipped with an Hg reservoir using pure Ne and Ar as the carrier gas, respectively. The temperature of the heated nozzle was kept at ca. 200 °C, which corresponds to a Hg vapor pressure of ca. 17 Torr (1 Torr=133.322 Pa). In order to prevent the formation of larger clusters, the stagnation pressures of Ne and Ar were kept below 6.5 and 1.5 atm, respectively. The pulsed nozzle adopted here was a fuel-injector with a tip orifice diameter of 0.8 mm, and was operated at 7 Hz. The background pressure in the chamber during the experiments was ca. 10^{-4} Torr.

When measuring the PHOFEX spectrum, HgNe or HgAr was excited into the $B^3\Pi_1$ state using the first UV laser light beam (ω_1: 252.5—253.9 nm); and the Hg(6^3P_1) photofragments produced via the repulsive part of the $B^3\Pi_1$ state potential were monitored by a second UV laser light beam (ω_2; 289.4 nm) by exciting Hg(6^3P_1) to Hg(8^3S_1). The two UV laser light beams were frequency-doubled outputs of two dye lasers (ω_1: Lambda Physik FL3002E; ω_2: Molectron DL-14P) simultaneously pumped by a XeCl excimer laser (Lambda Physik LPX105i). The frequency-doubling was performed using β-BaB_2O_4 and KDP crystals for ω_1 and ω_2, respectively. In high-resolution measurements, an intracavity etalon was inserted for the first dye laser for ω_1.

The two UV laser beams were counter-propagated and crossed at right angles with a free-jet 15 mm downstream from the nozzle orifice. The fluorescence emitted from the crossing region was detected by two photomultipliers placed in a direction perpendicular to both laser beams and the jet axis. A solar-blind type photomultiplier (Hamamatsu R166UH) was used to detect the fluorescence (ca. 250 nm) emitted from the $B^3\Pi_1$ state of HgRg; another (Hamamatsu R928) with an optical filter (Toshiba UV33) was used to detect emission in the visible and UV regions above ca. 330 nm. The fluorescence signals were amplified by a preamplifier (NF BX-31) and averaged by a boxcar integrator (Stanford SR250). In measurements of the LIF spectrum, we introduced only the ω_1 laser light, and scanned its wavelength while detecting the fluorescence using a solar-blind photomultiplier. In measurements of the LIF and PHOFEX spectra, the wavelength of the laser light for ω_1 was calibrated with respect to the LIF spectrum of I_2,[29] measured simultaneously. The wavenumber resolutions of the low- and high-resolution spectra were ca. 0.5 and ca. 0.08 cm^{-1}, respectively.

Results and Discussion

(i) PHOFEX Spectroscopy of HgNe. In Fig. 1, the low-resolution LIF (upper trace) and PHOFEX (lower trace) spectra of HgNe, measured simultaneously, are shown in the $B^3\Pi_1$–$X^1\Sigma^+$ band region. The LIF spectrum measured in the present study is consistent with that previously reported by Fuke et al.[1,2] and Yamanouchi et al.[3] In the LIF spectrum, the vibrational progression with only three distinct members, assigned to the $(v',v'')=(0,0)$, (1,0), and (2,0) transitions, converges to the dissociation limit located at ca. 39448 cm^{-1}. In the higher energy region above the threshold, there is a continuum part, indicating that the transition occurs to the repulsive part of the $B^3\Pi_1$ state potential.

The small peaks are identified in the PHOFEX spectrum at the same wavenumber positions where the (0,0) and (1, 0) transition peaks are observed in the LIF spectrum. These small peaks in the PHOFEX spectrum were ascribed to a leakage of the fluorescence emitted in the UV region through the optical filter which cuts most of the UV fluorescence, since they still exist with the same intensities, even when the probe laser is off.

By a comparison of the observed PHOFEX and LIF spectra, it can be noticed that the formation of the Hg(6^3P_1) photofragments gradually increases in the threshold region. In order to investigate this threshold behavior more precisely,

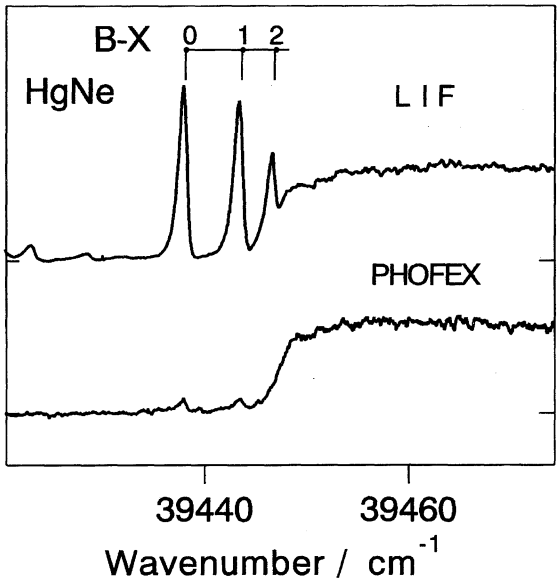

Fig. 1. The low-resolution LIF (upper trace) and PHOFEX (lower trace) spectra for the $B^3\Pi_1$–$X^1\Sigma^+$ band of HgNe.

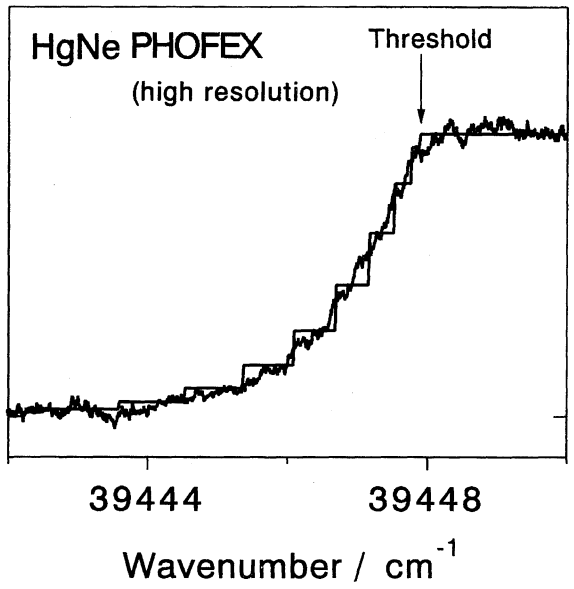

Fig. 2. The high-resolution PHOFEX spectrum of the $B^3\Pi_1$–$X^1\Sigma^+$ band of HgNe, and the simulated staircase spectrum. The rotational temperature of the simulated spectrum is 1.8 K.

PHOFEX measurements were performed with high resolution ($\Delta\nu\approx0.08$ cm^{-1}). The high-resolution spectrum shown in Fig. 2 exhibits a tail region extending 4—5 cm^{-1}.

This gradual increase in the threshold region of the PHOFEX spectrum can be interpreted consistently by taking account of the rotationally hot transitions. The dissociation threshold for the rovibronic transition to the continuum region of the $B^3\Pi_1$ state from a certain rotational level in the $X^1\Sigma^+$ state having a rotational quantum number, $J''=J$, should be shifted by $B''J(J+1)$ towards the lower energy side from the dissociation threshold for the transition from the $J''=0$ level in the $X^1\Sigma^+$ state, where B'' stands for the rotational constant for the $v''=0$ level of the electronic ground $X^1\Sigma^+$ state. It should be noted that (i) the observed PHOFEX spectrum is a superposition of the rovibronic transitions from the respective rotational levels in the $X^1\Sigma^+$ state to the $B^3\Pi_1$ state of HgNe, forming the $Hg(6^3P_1)$ photofragments, and that (ii) the transitions from the higher J'' levels have a lower threshold energy for the dissociation. Therefore, as the excitation energy increase in the threshold region of the PHOFEX spectrum, the threshold for the dissociation is reached in order from the high-J'' transitions to the low-J'' transitions; consequently, the PHOFEX intensity increases until the transition from the lowest $J''=0$ level begins to contribute to the photodissociation.

On the basis of the above consideration about the rotational effect, the threshold behavior of the observed PHOFEX spectrum was simulated by a trial-and-error procedure, in which the wavenumber of the dissociation threshold (ν_{th}) and the rotational temperature (T_R) were varied as two independent variable parameters. In the simulation of the PHOFEX spectrum, the shape of the Franck–Condon pattern for the rovibronic transitions to the continuum region was assumed to be a single-step staircase function, whose step height represents the statistical weight ($2J''+1$) of the rotational level of the electronic ground state. Since we are interested in the narrow tail region extending only 4—5 cm^{-1} just below the dissociation threshold, which is by far smaller than the range (ca. 110 cm^{-1}) of the smooth continuum region, the staircase function is expected to represent well the threshold behavior. Using the above single-step staircase FC pattern, the superpositions of the rovibronic transition intensities multiplied by a Boltzmann factor was taken to synthesize the PHOFEX spectrum.

Since the dissociation threshold (ν_{th}) determines the wavenumber position at which the PHOFEX intensity begins to drop and the rotational temperature (T_R) determines the wavenumber range of the tail region extending towards the lower energy region, these two parameters were optimized almost independently in the simulation of the PHOFEX spectrum. The best-fit simulated PHOFEX spectrum is compared in Fig. 2 with the observed spectrum. It can be seen in Fig. 2 that the simulated spectrum well reproduces the overall feature of the observed spectrum. From this analysis, $\nu_{th}=39447.9(3)$ cm^{-1} and $T_R=1.8(4)$ K were derived as optimized parameters, where the numbers in the parentheses represent the estimated limits of error.

In the tail region of the simulated PHOFEX spectrum in Fig. 2, there is a stair-case like structure, which cannot be clearly identified in the observed spectrum. In the simulated spectrum, each step in the staircase represents the opening or a lower J'' channel, causing dissociation. The disappearance of a clear staircase in the observed PHOFEX spectrum is ascribable to the existence of the six abundant isotope species of ^{m}Hg with m=198, 199, 200, 201, 202, and 204. As discussed by Yamanouchi et al.,[3] the A–X and B–X vibronic transitions of HgRg exhibit isotope splittings, mainly due to a volume isotope effect. The magnitudes of the isotope splitting between the lightest isotope (^{198}Hg) and the heaviest one (^{204}Hg) can be estimated to be at most 0.5 cm^{-1} in the B–X band,[3] and the splittings between adjacent isotope species are in the range of 0.05—0.20 cm^{-1}, which is comparable to the spacings between the steps. Therefore, the overlapping of the PHOFEX spectrum of the six isotope species of ^{m}HgNe may smear out the stepwise increase in the intensity of the PHOFEX spectrum. By meaning the PHOFEX spectrum of the single mass species of HgRg by a mass-resolved REMPI technique, a staircase-like structure could be identified, as predicted by the simulated spectrum.

By using Eq. 1 with a dissociation threshold of $\nu_{th}=39447.9(3)$ cm^{-1} and ν_{00}(HgNe)=39438.06(4) cm^{-1} of the $B^3\Pi_1$–$X^1\Sigma^+$ (0,0) band,[3] the dissociation energy (D_0) for the $B^3\Pi_1$ state was determined to be $D_0(B^3\Pi_1)=9.8(3)$ cm^{-1}. Then, as described in the introduction section, the dissociation energies of the $X^1\Sigma^+$ and $A^3\Pi_{0^+}$ states were derived straightforwardly to be $D_0(X^1\Sigma^+)=35.6(3)$ and $D_0(A^3\Pi_{0^+})=68.7(3)$ cm^{-1} from the dissociation energy of the $B^3\Pi_1$ state and ν_{00} of the $R^3\Pi_{0^+}$–$X^1\Sigma^+$ band.[3] Since the rotational band origin of the $B^3\Pi_1$–$X^1\Sigma^+$ (0,0) band reported by Yamanouchi et al.[3] was regarded as being that of the ^{200}HgNe species, the obtained dissociation threshold and dissociation energies

Table 1. Dissociation Energies, D_0 (cm^{-1}), of HgNe and HgAr in the $X^1\Sigma^+$, $A^3\Pi_{0^+}$, and $B^3\Pi_1$ States Determined from the Dissociation Thresholds for the $B^3\Pi_1$–$X^1\Sigma_0^+$ Bands[a)]

	HgNe	HgAr
$X^1\Sigma^+$	35.6(3)	123.7(5)
$A^3\Pi_{0^+}$	68.7(3)	348.8(6)
$B^3\Pi_1$	9.8(3)	61.8(5)

a) The dissociation thresholds for the $B^3\Pi_1$–$X^1\Sigma^+$ bands for HgNe and HgAr are 39447.9(3) and 39536.0(5) cm^{-1}, respectively.

correspond to those for the ^{200}HgNe isotope species. The determined dissociation energies of the $X^1\Sigma^+$, $A^3\Pi_{0^+}$, and $B^3\Pi_1$ states are summarized in Table 1.

It is possible that the dissociation threshold for each transition from the rotational level with a rotational quantum number of J'' in the electronic ground $X^1\Sigma^+$ state is shifted towards the higher energy side by the centrifugal barrier in the $B^3\Pi_1$ state. However, for the lower J' values in the electronic excited $B^3\Pi_1$ state, which were accessed in the present experimental condition, this centrifugal energy shift should be very small. Under the present ultracold ($T_R \approx 1.8$ K) expansion conditions, the populations of the rotational levels with $J''>5$ in the electronic ground $X^1\Sigma^+$ state are considerably small (<10%), from which transitions occur to the $J' \geq 5$ levels in the electronically excited $B^3\Pi_1$ state. Indeed, when the Morse potential function derived by Yamanouchi et al.[3)] is adopted, the height of the centrifugal barrier for $J'=5$ is only 0.22 cm^{-1}, measured from the dissociation limit of this Morse function. Furthermore, as shown in Fig. 2, the energy position where the intensity starts to fall off from the continuum level is clearly identified in the PHOFEX spectrum. Considering that this fall-off point corresponds with the dissociation threshold for the transition from the lowest $J''=0$ level in the electronic ground $X^1\Sigma^+$ state, the centrifugal energy shift affords only a negligible contribution to the dissociation threshold derived from the simulation described above.

In the LIF spectrum shown in Fig. 1, two weak bands were identified at 39423.1 and 39428.5 cm^{-1}, which were assigned, respectively, to the vibrational hot-band transitions, $B^3\Pi_1$–$X^1\Sigma^+$ (0,1) and (1,1), from the $v''=1$ level of the electronic ground $X^1\Sigma^+$ state. The (0,1) and (1,1) bands are located at 15.0 cm^{-1} below the (0,0) and (1,0) bands, respectively, indicating that the vibrational term value for the $v''=1$ level is 15.0 cm^{-1}. Therefore, the PHOFEX threshold for the hot band transition from $v''=1$ level in the X state should be located 15.0 cm^{-1} below the threshold ν_{th}=39447.9(3) cm^{-1} derived above for the transition from $v''=0$ level. However, as can be seen in Fig. 2, such a hot-band threshold was too weak to be identified in the observed PHOFEX spectrum. This means that no contribution is expected from the hot-band transitions to modify the threshold region of the PHOFEX spectrum.

From the determined dissociation energy, D_0=9.8(3) cm^{-1} for the $B^3\Pi_1$ state of HgNe, the dissociation energy (D_e) was estimated as $D_e=D_0+(1/2)\omega_e-(1/4)\omega_e x_e$=13.45(30) cm^{-1} using the Morse parameters ω_e=7.9 and $\omega_e x_e$=1.2 cm^{-1} determined previously by Yamanouchi et al.[3)] On the other hand, by using these Morse parameters, the dissociation energy (D_e) was predicted by the Morse equation to be $D_e=\omega_e^2/(4\omega_e x_e)$=13.00 cm^{-1}, which is in good agreement with D_e=13.45 cm^{-1} derived from D_0. This agreement indicates that the Morse function well describes the shape of the interatomic potential of the $B^3\Pi_1$ state of HgNe. The determined potential parameters for the $B^3\Pi_1$ state of HgNe are listed in Table 2 together with those determined from previous studies. The obtained dissociation energies (D_0 and D_e) for the $B^3\Pi_1$ state of HgNe are consistent with those estimated by Koperski et al.[15)] from a Birge–Sponer plot. However, the precision of these dissociation energies was considerably improved in the present study due to the direct high-resolution measurements of the photodissociation thresbold.

(ii) PHOFEX Spectroscopy of HgAr. Figure 3 shows

Table 2. Determined Potential Parameters of the $B^3\Pi_1$ States of HgNe and HgAr, and Comparisons with the Previous Studies

	ω_e / cm^{-1}	$\omega_e x_e$ / cm^{-1}	D_0 / cm^{-1}	D_e / cm^{-1}	R_e / Å
HgNe ($B^3\Pi_1$)					
This study	—	—	9.8(3)	13.45(30)	—
Fuke et al.[2)]	8.6	1.3	13	17	4.57
Yamanouchi et al.[3)]	7.9	1.2	11	13	4.92
Koperski et al.[15)]	7.7(4)	1.12(5)	9.7(7)	13.3(8)	4.71(1)
HgAr ($B^3\Pi_1$)					
This study	11.94(3)	0.594(3)	61.8(5)	67.62(50)	—
Fuke et al.[2)]	12.1	0.53	61	67	4.66
Yamanouchi et al.[3)]	11.5	0.63	57(4)	53	4.70
Krim et al.[13)]	11.2	0.6	—	—	—
Quayle et al.[14)]	12.4	0.59	—	72.02	—
Koperski et al.[15)]	12.7(2)	0.60(1)	61.0(10)	67.2(10)	4.47(1)

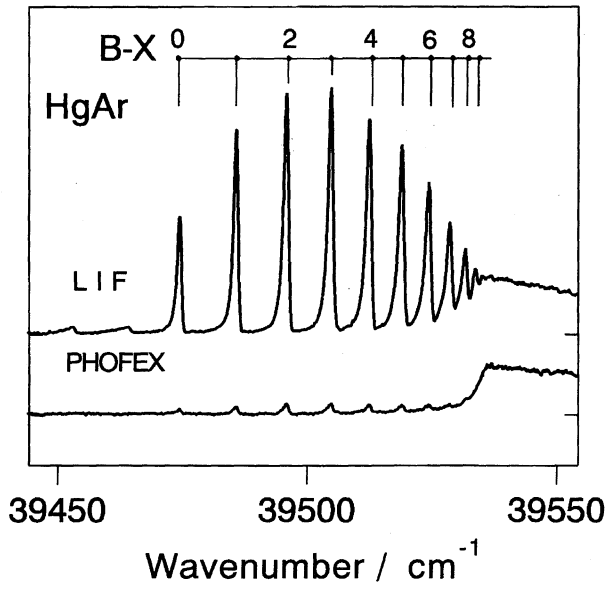

Fig. 3. The low-resolution LIF (upper trace) and PHOFEX (lower trace) spectra for the $B^3\Pi_1$–$X^1\Sigma^+$ band of HgAr.

the low-resolution LIF (upper trace) and PHOFEX (lower trace) spectra, which were simultaneously measured in the $B^3\Pi_1$–$X^1\Sigma^+$ band region of HgAr. The LIF spectrum measured in the present study is consistent with that reported previously by Fuke at al.[1,2] and Yamanouchi et al.[3] In the LIF spectrum, the relatively long vibrational progression has been identified with ten discernible transitions converging to the dissociation threshold located at ca. 39536 cm^{-1}. In the higher energy region above the threshold, there is a continuum part extending ca. 80 cm^{-1}, indicating that the transition occurs to the repulsive part of the $B^3\Pi_1$ state potential.

High-resolution measurements were performed for the (v', 0) vibronic bands for v'=0—8 in order to resolve their rotational structures. Although these rotational structures were consistent with the previous measurements by Yamanouchi et al.,[3] the vibrational assignments were off by one in the previous study. The rotational band origins and the observed rotational structure, labelled as the B–X(v',0) transition in a previous report by Yamanouchi et al.,[3] should be corrected to those for the B–X(v'+1,0) transition. The rotational band origin wavenumbers determined from a rotational analysis in the present study are listed in Table 3. From a Birge–Sponer plot of the observed band origins, the Morse potential parameters were determined to be ω_e=11.94(3) and $\omega_e x_e$=0.594(3) cm^{-1}. From a rotational contour analysis of the high-resolution LIF spectra of the $B^3\Pi_1$–$X^1\Sigma^+$ transitions, the rotational temperature was determined to be 3.0(2) K. The determined potential parameters for the $B^3\Pi_1$ state of HgAr are listed in Table 2 together with those determined in previous studies.

Table 3. Rotational Band Origins (cm^{-1}) for the $B^3\Pi_1$–$X^1\Sigma^+$ (v',0) Transitions of HgAr

v	Band origin
0	39474.23(4)
1	39485.57(4)
2	39495.75(4)
3	39504.74(4)
4	39512.49(4)
5	39519.10(4)
6	39524.51(4)
7	39528.66(4)
8	39531.76(4)

a) Numbers in parentheses represent estimated limits of error.

As in Fig. 1 for HgNe, the small peaks identified in the PHOFEX spectrum of HgAr at the same wavenumber positions where the discrete vibronic transition peaks are observed in the LIF spectrum were ascribed to a leakage of the fluorescence emitted in the UV region through the optical filter. The threshold behavior of the PHOFEX spectrum is more clearly seen in a high-resolution PHOFEX spectrum ($\Delta\nu\approx$0.08 cm^{-1}) given in Fig. 4, which shows that the tail region extends 4—5 cm^{-1}.

In order to interpret the threshold behavior of the PHOFEX spectrum, a trial-and-error simulation was performed by treating only the dissociation threshold (ν_{th}) as one variable parameter, while the rotational temperature (T_R) was fixed at T_R=3.0 K, which was determined by a simulation of the rotational structures of the B–X(v',0) discrete transitions, measured under the same experimental conditions as the PHOFEX spectrum. From the simulation, the threshold value, 39536.0(5) cm^{-1}, was determined for the B–X transition of HgAr.

By using Eq. 1 with a dissociation threshold of ν_{th}= 39536.0(5) cm^{-1} and ν_{00}(HgAr)=39474.23(4) cm^{-1} of the $B^3\Pi_1$–$X^1\Sigma^+$ (0,0) band, obtained in the present study, the dissociation energy (D_0) for the $B^3\Pi_1$ state was determined to be $D_0(B^3\Pi_1)$=61.8(5) cm^{-1}; the dissociation energies of the $X^1\Sigma^+$ and $A^3\Pi_{0^+}$ states were then derived straightfor-

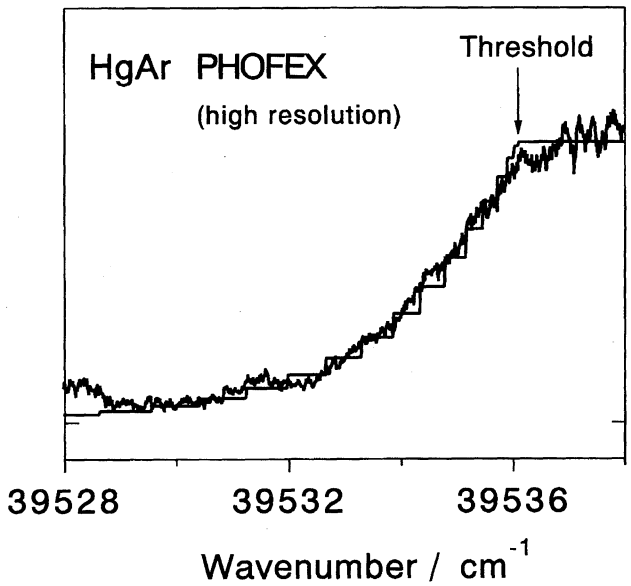

Fig. 4. The high-resolution PHOFEX spectrum of the $B^3\Pi_1$–$X^1\Sigma^+$ band of HgAr, and the simulated staircase spectrum. The rotational temperature of the simulated spectrum is 3.0 K.

wardly to be $D_0(X^1\Sigma^+)=123.7(5)$ and $D_0(A^3\Pi_{0^+})=348.8(6)$ cm^{-1} from the dissociation energy of the $B^3\Pi_1$ state and ν_{00} of the $R^3\Pi_{0^+}-X^1\Sigma^+$ band.[3] The determined dissociation energies of the $X^1\Sigma^+$, $A^3\Pi_{0^+}$, and $B^3\Pi_1$ states are summarized in Table 1.

Regarding the interatomic potential of the $B^3\Pi_1$ state of HgAr, the C_6 and C_8 potential terms were introduced to correctly describe the long-range behavior. Revisions of the potential parameters were recently attempted by Koperski[16] by using previous spectroscopic data. It would be worth mentioning here that the dissociation threshold, 39535.54(10) cm^{-1}, described by Lawrence et al.[17] as the beginning of the dissociation continuum, and that estimated as 39535.15 cm^{-1} by Koperski from a LeRoy–Bernstein plot, were all consistent with the threshold value of 39536.0 cm^{-1}, determined directly from the PHOFEX spectrum in the present study.

As discussed in Section (i) for HgNe, the centrifugal barrier shifts the threshold energies for the respective J'' channels in the PHOFEX spectrum. However, due to the heavier reduced mass for HgAr, the contribution from the centrifugal barrier was found to be smaller than that in HgNe under jet-cooled conditions in the present study. Therefore, for the same reasons as those described for HgNe, the effect of the centrifugal barrier can be neglected in the above simulation to derive the dissociation threshold. In the LIF spectrum shown in Fig. 3, two weak bands were identified at 39453.1 and 39464.4 cm^{-1}, which were assigned, respectively, to the vibrational hot-band transitions, $B^3\Pi_1$–$X^1\Sigma^+$ (0,1) and (1, 1), from the $v''=1$ level of the electronic ground $X^1\Sigma^+$ state. The (0,1) and (1,1) bands are located at 21.7 cm^{-1} below the (0,0) and (1,0) bands, respectively, indicating that the vibrational term value for the $v''=1$ level is 21.7 cm^{-1}. Similar to the HgNe case, the hot-band contribution was found to be neglibly small in the threshold behavior of the PHOFEX spectrum.

Summary

PHOFEX (photofragment excitation) spectroscopy was for the first time applied to determine the spectroscopic dissociation energies (D_0's) of HgNe and HgAr in their low-lying electronic states, i.e. $X^1\Sigma^+$, $A^3\Pi_{0^+}$, and $B^3\Pi_1$ states. From a simulation of the threshold behavior of the high-resolution PHOFEX spectra of the $B^3\Pi_1$–$X^1\Sigma^+$ bands of HgNe and HgAr by monitoring the $Hg(6^3P_1)$ photofragments, the dissociation thresholds for the $B^3\Pi_1$ states were determined with high-precision to be 39447.9(3) and 39536.0(5) cm^{-1} for HgNe and HgAr, respectively. From theses thresholds, the dissociation energies (D_0's) of the $B^3\Pi_1$ states of HgNe and HgAr were determined to be $D_0(B^3\Pi_1;\ HgNe)=9.8(3)$ and $D_0(B^3\Pi_1;\ HgAr)=61.8(5)$ cm^{-1}, respectively. This direct determination of the dissociation energies of the $B^3\Pi_1$ states led to a determination of the D_0's for the $X^1\Sigma^+$ and $A^3\Pi_{0^+}$ states; $D_0(X^1\Sigma^+;\ HgNe)=35.6(3)$, $D_0(X^1\Sigma^+;\ HgAr)=123.7(5)$, $D_0(A^3\Pi_{0^+};\ HgNe)=68.7(3)$, and $D_0(A^3\Pi_{0^+};\ HgAr)=348.8(6)$ cm^{-1}. The present determination of the dissociation energies of HgNe and HgAr demonstrates that PHOFEX spectroscopy, which has been applied to investigate photodissociation reactions, is also an efficient approach to determine the spectroscopic dissociation energies (D_0's) of simple molecules.

The present study was supported in part by Grants-in-Aid from the Ministry of Education, Science, Sports and Culture (Nos. 05453016, 07240106, and 08640636).

References

1) K. Fuke, T. Saito, and K. Kaya, *J. Chem. Phys.*, **79**, 2487 (1983).
2) K. Fuke, T. Saito, and K. Kaya, *J. Chem. Phys.*, **81**, 2591 (1984).
3) K. Yamanouchi, S. Isogai, M. Okunishi, and S. Tsuchiya, *J. Chem. Phys.*, **88**, 205 (1988).
4) K. Yamanouchi, J. Fukuyama, H. Horiguchi, S. Tsuchiya, K. Fuke, T. Saito, and K. Kaya, *J. Chem. Phys.*, **85**, 1806 (1985).
5) M. Okunishi, H. Nakazawa, K. Yamanouchi, and S. Tsuchiya, *J. Chem. Phys.*, **93**, 7256 (1990).
6) T. Tsuchizawa, K. Yamanouchi, and S. Tsuchiya, *J. Chem. Phys.*, **89**, 4646 (1988).
7) M. C. Duval, C. Jouvet, and B. Soep, *Chem. Phys. Lett.*, **119**, 317 (1985).
8) M. C. Duval, O.B. d'Azy, W. H. Breckenridge, C. Jouvet, and B. Soep, *J. Chem. Phys.*, **85**, 6324 (1986).
9) W. H. Breckenridge, M. C. Duval, C. Jouvet, and B. Soep, *Chem. Phys. Lett.*, **122**, 181 (1985).
10) R. van Zee, S. C. Blankespoor, and T. S. Zwier, *Chem. Phys. Lett.*, **158**, 306 (1989).
11) M. Okunishi, K. Yamanouchi, and S. Tsuchiya, *J. Chem. Phys.*, **97**, 2305 (1992).
12) J. Zuniga, A. Bastida, A. Requena, N. Halberstadt, and J. A. Beswick, *J. Chem. Phys.*, **98**, 1007 (1993).
13) L. Krim, P. Qiu, C. Jouvet, C. L. -Dedonder, J. G. McCaffrey, B. Soep, D. Solgadi, O. B. d'Azy, P. Ceralolo, N. D. Hung, M. Martin, and Y. Meyer, *Chem. Phys. Lett.*, **200**, 267 (1990).
14) C. J. K. Quayle, I. M. Belle, E. Takacs, X. Chen, K. Burnett, and D. M. Segal, *J. Chem. Phys.*, **99**, 9608 (1993).
15) J. Koperski, J. B. Atkinson, and L. Krause, *Chem. Phys.*, **186**, 401 (1994).
16) J. Koperski, *J. Chem. Phys.*, **105**, 4920 (1996).
17) S. J. Lawrence, D. N. Stacey, I. M. Bell, and K. Burnett, *J. Chem. Phys.*, **104**, 7860 (1996).
18) M. Okunishi, K. Yamanouchi, K. Onda, and S. Tsuchiya, *J. Chem. Phys.*, **98**, 2675 (1993).
19) K. Onda, K. Yamanouchi, M. Okunishi, and S. Tsuchiya, *J. Chem. Phys.*, **101**, 7290 (1994).
20) K. Onda and K. Yamanouchi, *J. Chem. Phys.*, **102**, 1129 (1995).
21) K. Onda and K. Yamanouchi, *J. Chem. Phys.*, **104**, 9376 (1996).
22) K. Onda, T. Tasaka, A. Hishikawa, and K. Yamanouchi, in "Structure and Dynamics of Clusters," ed by T. Kondow and K. Kaya, Universal Academy Press (1996), p. 347.
23) C. E. Moore, "Atomic Energy Levels," U. S. GPO, Washington, D. C. (1971), Vol. III.
24) J. Miyawaki, K. Yamanouchi, and S. Tsuchiya, *Chem. Phys. Lett.*, **180**, 287 (1991).
25) J. Miyawaki, K. Yamanouchi, and S. Tsuchiya, *J. Chem.*

Phys., **99**, 254 (1993).
26) C. D. Pibel, K. Ohde, and K. Yamanouchi, *J. Chem. Phys.*, **101**, 836 (1994).
27) K. Yamanouchi, K. Ohde, A. Hishikawa, and C. D. Pibel, *Bull. Chem. Soc. Jpn.*, **68**, 2459 (1995).
28) A. Hishikawa, K. Ohde, R. Itakura, S. Liu, K. Yamanouchi, and K. Yamashita, *J. Phys. Chem.*, **101**, 694 (1997).
29) J. Cariou and P. Luc, "Atlas du Spectre d'Absorption de la Molecule de Tellure," Laboratoire Aime-Cotton, CNRS II, Orsay (1980).